300 fs pulsed laser ablation of Al2O3 ceramic and introduction of a predictive model

Author(s):
Weixler, Jodok; Zweifel, Marc; Wegener, Konrad

Publication date:
2022-05

Permanent link:
https://doi.org/10.3929/ethz-b-000542568

Originally published in:
Materials & Design 217, https://doi.org/10.1016/j.matdes.2022.110614

Materials & Design 217 (2022) 110614

Contents lists available at ScienceDirect

Materials & Design

journal homepage: www.elsevier.com/locate/matdes

300 fs pulsed laser ablation of Al_2O_3 ceramic and introduction of a predictive model

Jodok Weixler *, Marc Zweifel, Konrad Wegener

Institute of Machine Tools and Manufacturing, ETH Zürich, Leonhardstrasse 21, 8092 Zürich, Switzerland

HIGHLIGHTS

- The surface topography after pulsed laser ablation of alumina ceramic can be predicted accurately.
- Higher ablation efficiency of alumina ceramic is achieved at slower scan speeds.
- The authors hope that the results will be useful for the design of laser ablation processes on alumina components.

GRAPHICAL ABSTRACT

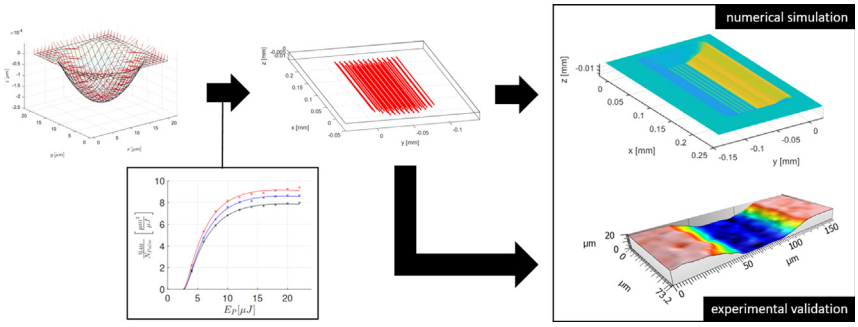

ARTICLE INFO

Article history:
Received 30 November 2021
Revised 29 March 2022
Accepted 30 March 2022
Available online 5 April 2022

Keywords:
Predictive calculation routine
Laser ablation of Al_2O_2 ceramic
Neuenschwander model

ABSTRACT

In this study a calculation routine for predicting the ablation topography considering the angle of incidence and the evolution of the ablated surface pulse by pulse is presented and applied. Laser processing of Al_2O_3 ceramic is studied by the ablation of single craters as well as by macroscopic ablation pockets for a pulse duration of 300 fs at a wavelength of 515 nm. The threshold fluence is determined and compared for different process configurations and it is demonstrated that lower scanspeed leads to a higher removal rate. The accuracy of this method is evaluated in an ablation experiment. The presented method is useful for predicting the surface topography in order to optimize the scanpath or to apply machine learning algorithms.

1. Introduction

Alumina Ceramics (Al_2O_3) are applied for parts with high requirements regarding temperature stability, electrical isolation, corrosion resistance, wear resistance and hardness. Due to the very high hardness in combination with a low friction coefficient, Al_2O_2 is applied for components in textile industry such as threat guides as well as for medical implants.

Ultra short pulsed (USP) laser processing is a versatile manufacturing technology used for micro processing. It can be applied for cutting, drilling, surface treatment and generation of complex 3D shapes. This manufacturing technology has several advantages such as elimination of contamination, of tool wear and process forces and a very dynamic beam deflection leading to high surface processing speeds. The characteristics of femtosecond ablation of Al_2O_2 have been studied in several publications [1–3]. Ashkenasi et al. studied the ablation threshold of Al_2O_2 at a wavelength of 800 nm for different pulse durations ranging from 200 fs up to 4.5 ps for different number of pulses. A pronounced decrease of the threshold fluence with increasing the number of pulses is observed especially within the first 25 pulses. For a pulse duration of 200 fs the threshold fluence is determined to be 1.3 ± 0.1 J cm^{-2} for an infinite number of overlapping pulses. In the publication of

* Corresponding author.
E-mail address: weixler@iwf.mavt.ethz.ch (J. Weixler).

https://doi.org/10.1016/j.matdes.2022.110614

Perrie et al. [1] the ablation characteristic of Al_2O_2 using a pulse duration of 180 fs at a wavelength of 775 nm is studied. An ablation rate of $25 < V < 900\ \mu m^3$ per pulse for a pulse fluence between 1.4 J cm^{-2} and 21 J cm^{-2} is determined. It is reported that processing at a fluence of 1.4 J cm^{-2}, just above the ablation threshold estimated to be at 1.1 J cm^{-2}, the surface roughness can be reduced slightly from $R_a = 0.79 \pm 0.07\ \mu m$ down to $R_a = 0.64 \pm 0.07\ \mu m$. In the study of Kim et al. [3] the threshold fluence of Al_2O_2 is studied for processing at a pulse duration of 185 fs and a wavelength of 785 nm. The single pulse ablation threshold is determined to be 5.65 J cm^{-2} with an incubation factor S = 0.7. This corresponds to an ablation threshold of 1.42 J cm^{-2} and 1.15 J cm^{-2} for a number of 100 and 200 overlapping pulses, respectively. In the present study, the ablation characteristics of Al_2O_2 for a wavelength of 515 nm and a pulse duration of 300 fs are studied. Furthermore, the capabilities regarding surface texturing are studied.

USP lasers are applied for 2D applications such as surface texturing, drilling and cutting. In the case of 3D bulk removal for free-form shape generation, process development is getting more difficult. It is realized with a high degree of experimental work and know-how of experts. This is due to the complex nature of the laser ablation process itself. In conventional machining such as milling, drilling and grinding, the removed volume is given by the interaction volume between tool and workpiece. In laser machining, the removed material depends on the energy density function of the laser beam as well on the optical and physical properties of the material and the geometrical conditions on the workpiece such as oblique incidence and shadowing effects. On top of that, the energy density function changes on a very short timescale (<1 ps) to very high intensities (> 1 PW mm^{-2}) leading to highly non-linear material behaviour.

However, the state of the art for path planning of laser ablation is given by a slicing approach like it is applied in conventional machining by using simplified parameters such as track width, removal depth, scanspeed, power and repetition rate. These parameters are determined in fundamental experiments, prior to the slicing operation. The real removal rate in laser ablation changes if another scanstrategy is selected, or if one of the parameters are modified, such as scanspeed or pulse repetition rate. This complex interaction between parameters and ablation leads to high requirements in expert know-how for process development in laser ablation.

Simulation of USP laser ablation can be done on different scales. On the single pulse scale, the multiple rate equation model is used to predict optical properties and the ablation threshold [4]. Molecular dynamic simulations provide important information on the mechanics of the material transformation under conditions of strong superheating [5]. Simulation of an industrial ablation process with a duration of 1 min would require the calculation of several million single pulse events. Due to huge amount of computation time needed, this approaches are not applicable for simulating an industrial laser ablation operation or for virtual process development.

In order to overcome this limitation, a method for simulating the surface topography evolution was presented in 2014 [6] and also applied in 2020 [7]. The prediction of crater depth in polycrystalline diamond (PCD) within 9.4% deviation from the experiment was demonstrated whereas in [7] a deviation of 30% from the experiment is reported for predicting the ablation in nano PCD. The major reason for the deviation between simulation and experiment lies in the experimental conditions such as repetition rate, spot size and scanspeed in which the threshold fluence and penetration depth are determined. Following this, the suitable determination of the effective threshold fluence and penetration depth is the key to achieve accurate simulation results for predicting the surface topography for a wide range of different laser scan strategies.

Since the beginning of laser ablation, empirical models are used in order to understand the ablation process not only for the single pulses but also for an industrial relevant macroscopic ablation volume. The model for describing the relation of ablation depth d as a function of the pulse fluence F and the ablation threshold F_{th} is the well known equation:

$$d(F) = \delta \cdot ln(F/F_{th}) \tag{1}$$

A method for determining both, the waist radius of a Gaussian beam and the threshold fluence in an experimental approach was presented [8,9]. In order to apply the logarithmic ablation model more accurately and on an industrial scale, several extensions have been made. These modeling extensions are used for both determination of the process constants based on single pulse experiments and prediction of ablation depth by knowing the process constants. An extension to distinguish between different energy regimes is applied frequently [10–13]. Furthermore, an extension which describes the threshold fluence F_{th} for the ablation depending on the number of overlapping pulses N for dielectrics [14–16] and metals [9,17] can be found as follows:

$$F_{th}(N) = F_{th}(1) \cdot N^{S-1} \tag{2}$$

$$F_{th}(N) = F_{th}(\infty) + [F_{th}(1) - F_{th}(\infty)] \cdot exp[-k(N-1)] \tag{3}$$

In order to find a model for macroscopic laser ablation volumes, the calculation of the energy specific ablation volume was introduced in [18]. By fitting the experimentally determined ablation volume for a given parameter set into this calculation model, the effective threshold fluence and effective penetration depth need to be determined [19]. This approach brings high applicability for macroscopic experiments, because the multi-pulse effects automatically are taken into account during determination of the process constants. In order to consider angle dependent effects, an extension was made and validated for tungsten carbide and dielectric materials in [20,21].

2. Modeling method

In the following, the calculation routine for predicting the ablation depth is explained in detail. The model requires several input definitions. First, the energy distribution of the laser beam applied on the work piece is defined by providing pulse energy as well as the spatial and longitudinal beam profile. For a Gaussian beam the fluence distribution F as a function of the radius r and the distance from the focal plane z is given by

$$F(r,z) = \frac{2E_p}{\pi\omega(z)^2} \cdot exp\left(\frac{-2r^2}{\omega(z)^2}\right) \tag{4}$$

$$\omega(z)^2 = \omega_0^2\left(1 + \frac{z^2}{z_R^2}\right) \tag{5}$$

with the beam radius $\omega(z)$, the beam waist radius ω_0, the pulse energy E_p and the Rayleigh length z_R. The Rayleigh length is defined by the optical aperture M^2 as follows.

$$z_R = \frac{\pi \cdot \omega_0^2}{\lambda \cdot M^2} \tag{6}$$

It is possible to implement any laser beam profile besides the Gaussian shape in the calculation routine. Second, the workpiece geometry is be defined. In this predictive calculation, the surface is defined as a even spaced grid with custom size and resolution. The grid is defined by the three matrices S_x, S_y and S_z.

$$\boldsymbol{S_x} = \begin{bmatrix} x_{11} & x_{12} & \dots & x_{1n} \\ x_{21} & x_{22} & & \\ \vdots & & \ddots & \\ x_{m1} & & & x_{mn} \end{bmatrix}$$
$$\boldsymbol{S_y} = \begin{bmatrix} y_{11} & y_{12} & \dots & y_{1n} \\ y_{21} & y_{22} & & \\ \vdots & & \ddots & \\ y_{m1} & & & y_{mn} \end{bmatrix} \quad (7)$$
$$\boldsymbol{S_z} = \begin{bmatrix} z_{11} & z_{12} & \dots & z_{1n} \\ z_{21} & z_{22} & & \\ \vdots & & \ddots & \\ z_{m1} & & & z_{mn} \end{bmatrix}$$

Any geometric shape can be created or directly imported from measurements. The properties of the material such as threshold fluence and penetration depth need to be defined in this step as well.

Third, the deflection of the laser beam relative to the substrate is defined. Taking into account the laser beam trajectory, scan speed and pulse repetition rate, a list of laser pulse coordinates is generated.

$$\boldsymbol{L} = \begin{bmatrix} x_1 & x_2 & \dots & x_n \\ y_1 & y_2 & \dots & y_n \\ z_1 & z_2 & \dots & z_n \end{bmatrix} \quad (8)$$

With this input definitions, the calculation routine can be executed. The fluence distribution is calculated based on Eq. (4) and (5). For the inclination angle the normal vector of the surface for each element is considered. In Fig. 2 and 3 the normal vectors for each mesh element are illustrated for the surface after a single pulse and after multiple pulses, respectively.

$$\underline{n} = \begin{bmatrix} n_x \\ n_y \\ n_z \end{bmatrix} \quad (9)$$

$$\theta_i = arccos\left(\frac{n_z}{\sqrt{n_x^2 + n_y^2 + n_z^2}}\right) \quad (10)$$

The resulting fluence distribution F_r on the surface is calculated for each element by the angle θ_i between normal vector of the surface and the beam propagation axis, which is assumed to be z.

$$F_r(i) = F(i) \cdot cos\,\theta_i \quad (11)$$

For considering the angle dependent absorption F_r is multiplied with the effective absorption coefficient $A(\theta)$. The determination of effective process coefficients for dielectrics is described in a previous publication [21].

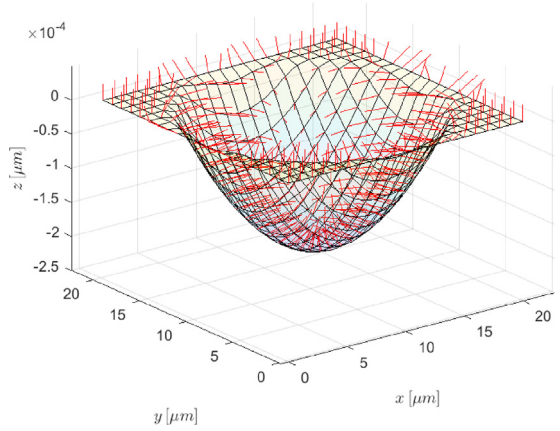

Fig. 2. Illustration of the normal vectors (red) calculated for each mesh point for a single pulse crater.

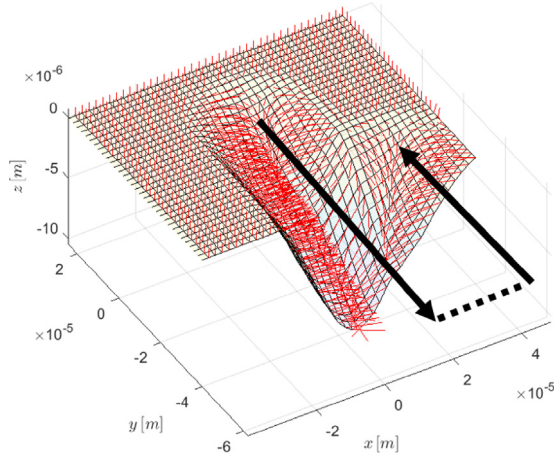

Fig. 3. Illustration of the normal vectors (red) calculated for each mesh point for a multipulse simulation along the scanpath (black).

With these definitions and calculations the ablation calculation can be performed for each element using the logarithmic ablation law.

$$\Delta z_i = \delta_{eff} \cdot ln\left(\frac{F(i) \cdot cos\,\theta_i}{F_{th,eff}}\right) \quad (12)$$

Using this routine leads to a calculation of one pulse event after another like a mathematical row. Thereby the surface normal vector matrix is recalculated again after each pulse. In this way the geometrical effects between the pulses are taken into account.

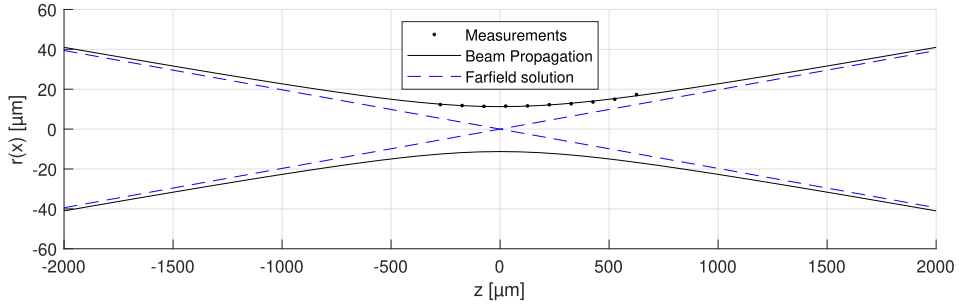

Fig. 1. Beamprofile close to the focal plane, measured at 10 positions along the propagation axis using a beam camera. $\omega_0 = 11.3$ µm, $z_r = 571.3$ µm.

Table 1
Laser beam characteristics.

Wavelength	pulse width (FWHM)	Focal length	ω_0 $(1/e^2)$	Polarization
515 nm	300 fs	163 mm	11.3 µm	circular

Table 2
Process parameters for the diameter regression (1) and the macroscopic ablation experiment (2). The process parameter N indicates the number of pulses on the same crater in experiment (1) and the number of passes in experiment (2).

Experiment	E_p	f_{rep}	N	v_s	Line distance
(1)	10–25 µJ	0.1 kHz	2–512	1 m s^{-1}	-
(2)	4–22 µJ	400 kHz	40	1, 1.5, 2 m s^{-1}	5 µm

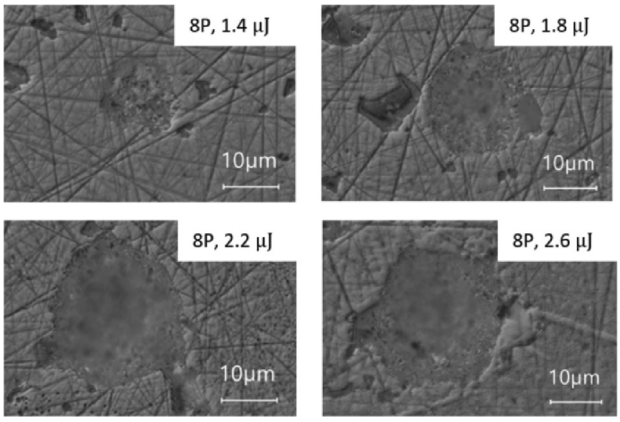

Fig. 4. Microscopic images of the ablated craters after 8 pulses in Al_2O_3 with a pulse duration of 300 fs at a wavelength of 515 nm at circular polarisation for the diameter regression experiment.

3. Experimental

The laser used for the experiments is a frequency doubled Yb:YAG laser emitting a linearly polarized beam at a wavelength of 515 nm with a pulse duration of 300 fs. The specifications of the laser source are given in Table 1. The beam is transformed to circular polarisation by placing a $\lambda/4$ plate into the beam-path in order to eliminate effects dependent on the scanning direction. A galvanometer scanhead is used for the beam deflection in X and Y direction and the beam is focused by a telecentric f-theta lens. The beam waist radius is measured to be 11.3 µm. The beam is characterized by the values described in Fig. 1. The mechanical stages as well as the scanner motion is controlled by the Aerotech Software A3200. The parameter studies as well as the ablation experiments are carried out on Al_2O_3 99.8 samples with a grain size of 5 µm from Heberlein AG. The processed surface is analysed by confocal microscopy.

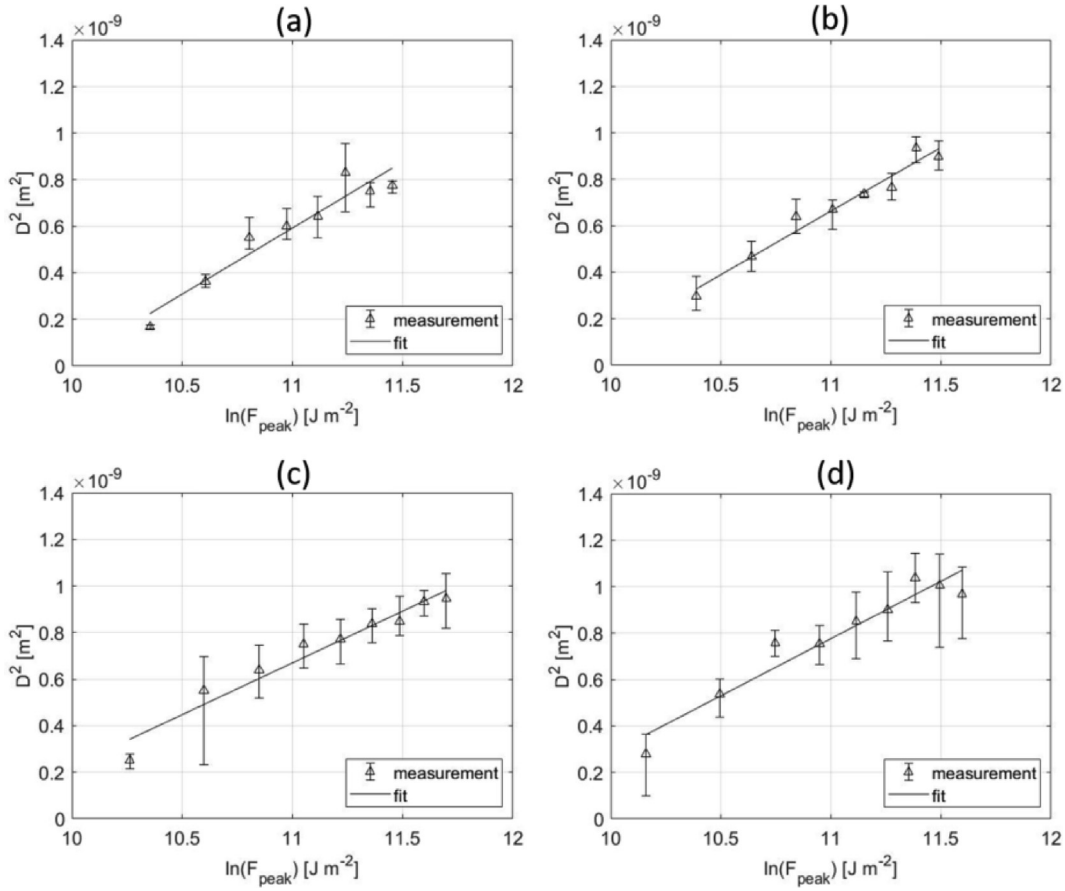

Fig. 5. Plot of D^2 versus logarithmic peak fluence of the laser pulse for 8 (a), 16 (b), 32 (c) and 64 pulses (d) as an average value of 4 measurements. The bars represent the minimum and the maximum value of each measurement.

In the pre-study the threshold fluence is determined applying two different approaches in order to evaluate the applicability of each method for the predictive calculation. In the first step, the threshold fluence is determined using the diameter regression method [9,8]. The experiment is done for different number of pulses ranging from 2–512 at a repetition rate of 0.1 kHz. The ablation threshold as a function of the number of pulses N applied is described by the exponential model (see Eq. 3). In the next step the effective threshold fluence and penetration depth are determined applying the Neuenschwander model [19,22]. The lateral size of the pockets for the Neuenschwander method is 1 mm × 1 mm and the scanning direction is rotated by an angle of 23° after each layer. The experiment applying the Neuenschwander model is performed at different scanspeeds. The parameters used for the diameter regression method (experiment 1) and the Neuenschwander method (experiment 2) are described in Table 2.

The surface roughness of the pockets ablated is evaluated by the confocal microscope Leica DCM 3D. The Sa value is calculated by the Leica Map software.

In the second step, the parameter set is chosen resulting in a good ratio of removal rate and surface quality. The target geometry is created in a CAD volume. The NC Code is generated by using the custom built slicing routine in MATLAB. In order to test if the NC Code leads to the target ablation volume, the NC Code is executed in a custom calculation routine for ablation, described in the previous section. The ablation depth is calculated pulse by pulse for every mesh point considering the logarithmic ablation law and the angle of incidence. The target depth of ablation is 15 µm. In the next step the ablation experiment is performed using the virtually tested scanstrategy. The ablation result is analyzed using confocal microscopy and compared to the simulated ablation profile.

Finally, the accuracy of the predictive model is studied by comparing the calculated ablation depth to the ablation depth of the final shape measured with the confocal microscope Leica DCM 3D.

4. Results and discussion

The craters from the diameter regression are shown in Fig. 4. It can be seen that the craters are not perfectly circular. The average diameter is determined from 5 measurements. In Fig. 5 the squared values of the diameter measurements for 8, 16, 32 and 64 pulses are plotted against the logarithmic peak fluence. From the single pulse experiments a threshold fluence of 0.44 J cm^{-2} for the first pulse is determined with an incubation factor of k = 0.157 and a threshold fluence for an infinite number of pulses of 0.14 J cm^{-2} (see Fig. 6). A saturation of the threshold fluence after the first 50 pulses can be observed according to the incubation model introduced in the previous section. The treshold fluence is 3 times higher for the first pulse compared to the threshold fluence for an infinite number of pulses. For the determination of the threshold fluence measuring the ablation pockets and applying the Neuenschwander model, the energy specific ablation volume per pulse is plotted in Fig. 7. It can be observed, that changing the pulse to pulse distance by increasing the scanspeed while leaving the repetition rate constant leads to a lower ablation rate. For a pulse energy of 10 µJ the ablation rate decreases by 16.3% by changing the scanspeed from 1 m s^{-1} to 2 m s^{-1}. This effect is evident for the whole range of tested pulse energies. A maximum peak in the ablation efficiency cannot be determined, as it does not decrease within the tested range of up to 22 µJ which corresponds to a pulse fluence of 62 J cm^{-2}.

The effective threshold fluence in combination with the effective penetration depth is determined by fitting the data to the Neuenschwander model [19]. As the ablation rate changes for a different pulse to pulse distance, the effective parameters change as

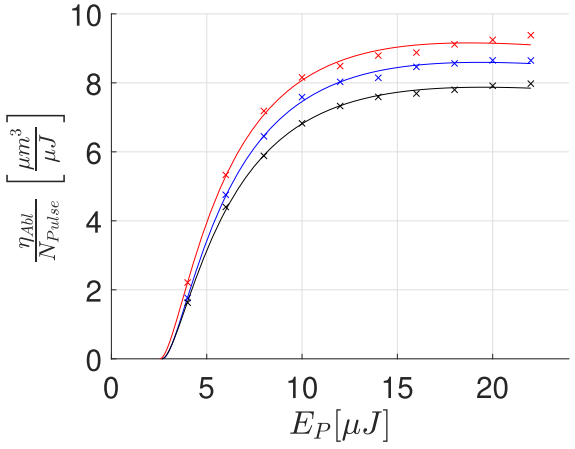

Fig. 7. Experimentally determined ablation efficiency per pulse for three different scanspeeds and corresponding fit of the Neuenschwander model. red: 1 m s^{-1}, blue: 1.5 m s^{-1}, black: 2 m s^{-1}.

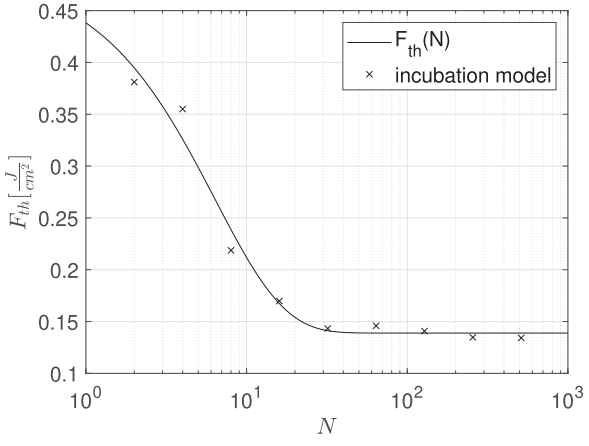

Fig. 6. Results of the diameter regression method. Threshold fluence as a function of the number of pulses N applied for each crater at a repetition rate of 0.1 kHz and the corresponding fit curve of the exponential model for incubation. $F_{th,1} = 0.44$ J cm^{-2}, $F_{th,inf} = 0.14$ J cm^{-2}, $k = 0.157$.

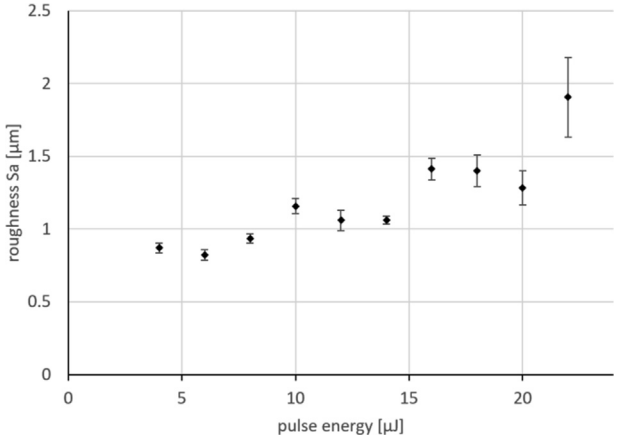

Fig. 8. Measured Sa value at the bottom of the ablation pockets machined at a scanspeed of 1 m s^{-1} determined for an area of 0.5 mm × 0.5 mm and corresponding error bars.

well. For a scanspeed of 1 m s^{-1} the threshold fluence of 0.71 J cm^{-2} and a penetration depth of 243 *nm* is determined. Comparing this effective threshold fluence to the one determined by the diameter regression method (see Fig. 4), a big difference can be observed. In the second step, the surface roughness of the pockets, ablated at a scanspeed of 1 m s^{-1} is evaluated in Fig. 8. There is a trend that for an increased energy the Sa value increases. For a pulse energy of 10 µJ and higher, a Sa value higher than 1 µm is determined.

The demonstrator part is manufactured using a pulse energy of 8 µJ, a scanspeed of 1 m s^{-1} and a hatch distance Δh of 6.5 µm with unidirectional orientation along the x-axis. In order to ablate the target profile for the application of the Al_2O_3 specimen without several experimental iterations, the NC Code was executed in the calculation routine described in the previous section. The resolution of the mesh is chosen to be 1 µm in the x and y direction. The laser beam parameters are defined according to Fig. 1. Regarding the material parameters, the effective threshold fluence and effective penetration depth determined for a scanspeed of 1 m s^{-1} are used. The optimized scanpath used for the calculation routine is plotted in Fig. 9. The calculation of the 3564 laser spot positions which contain approximately 400 mesh points, leads to 1.4 million calculation steps each including the normal vector calculation and ablation depth calculation, takes 1.9 s on a single core of an Intel Core i7-7700 CPU. The surface of the predicted surface with the optimized scanstragegy is plotted in Fig. 10. The corresponding measurement of the ablated sample is shown in Fig. 11. On the 3D view of the measurement the surface reveals a high waviness. In order to evaluate the agreement between the calculated surface and the experiment, a crosssection of both surfaces is plotted in Fig. 12. It can be seen that the ablation depth at the bottom of the groove is in good agreement with the calculated prediction. But the measured profile (red) reveals an stochastic waviness which could occur from the boundary of the grains which are in the order of 5 µm in diameter.

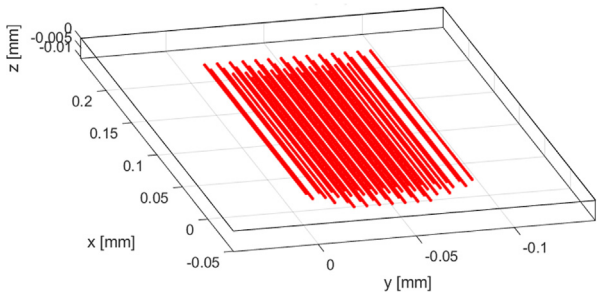

Fig. 9. Plot of the optimized scanpath. The resulting laser spot positions are plotted by each individual point.

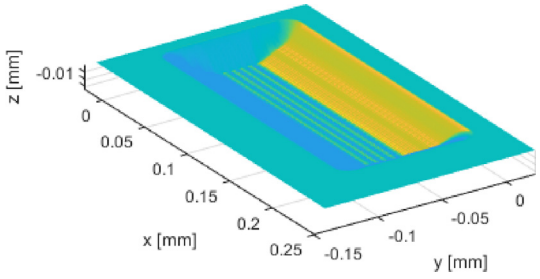

Fig. 10. Plot of the predicted surface topography calculated with the optimized scan-strategy in Fig. 7 and the process parameters E_p=8 µJ, v_s=1 m s^{-1} and Δh = 6.5 µm.

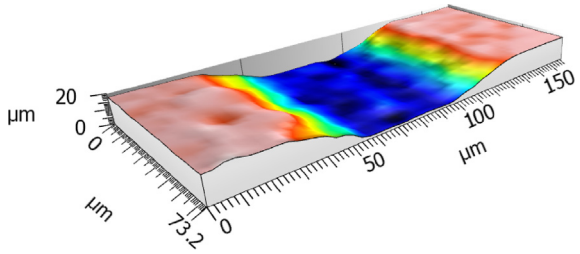

Fig. 11. 3D plot of the surface ablated using the final process parameters E_p=8 µJ, v_s=1 m s^{-1} and Δh = 6.5 µm. Measured by confocal microscopy at a magnification of x10 leading to a spatial resolution of 1.7 µm.

5. Conclusion

In this study a numerical prediction of the surface topography in USP laser ablation using empirical parameters is demonstrated. The procedure is applied for laser ablation of sintered Al_2O_3 samples using a 300 fs pulsed laser at a wavelength of 515 nm. In contrast to the threshold fluence determined in by the diameter regression method, the value determined by the Neuenschwander method $F_{th} = 0.71\,\mathrm{J\,cm^{-1}}$ is significantly higher. This value is comparable to $F_{th} = 0.69\,\mathrm{J\,cm^{-1}}$ obtained in a study using a 120 ps pulsed laser at a wavelength of 825 nm to machine alumina [18]. For a laser process at 300 fs at 1030 nm with N = 100 overlapping pulses on alumina $F_{th} = 1\,\mathrm{J\,cm^{-1}}$ was determined [23]. This implies that the threshold fluence of alumina is very sensitive to the wavelength applied.

Furthermore, the influence of the pulse to pulse distance on the ablation rate is studied by changing the scanspeed. The results show, that in the case of alumina, the ablation efficiency increases for lower scanspeeds. This observation is in accordance with the results of a recent study [23]. This effect might be caused either by incubation effects for more overlapping pulses or by a different contact angle of the laser beam which results from the higher track removal depth resulting from a smaller pulse to pulse distance. In the validation experiment a good agreement between simulation and experiment can be observed. The deviations might be the result of the microscopic properties of the grain boundaries which are in the order of 5 µm in diameter. This leads to the conclusion that numerical prediction of surface topography using empirical parameters determined by the Neuenschwander model is a useful approach to virtually test and optimize different scan strategies. In order to consider the scanspeed dependent effects, it might be use-

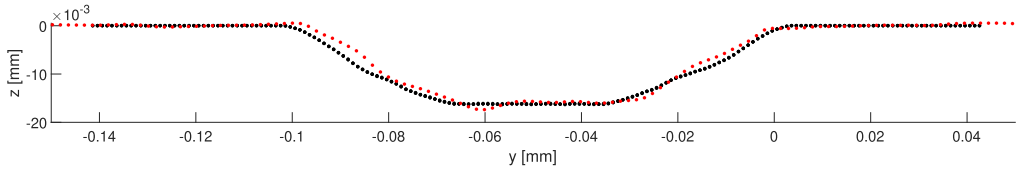

Fig. 12. Comparison of laser irradiation experiment and calculation. Cross section of the predicted surface (black) of Fig. 10 along the y axis in comparison to the measured profile (red) of the irradiation experiment from Fi.g. 9.

ful to introduce a parameter to enable an accurate predictive calculation for a range of scanspeeds. In the next step this approach needs to be applied also for other laser wavelengths and pulse durations as well as for different materials. For this, the empirical parameters need to be determined as demonstrated in this study using the Neuenschwander model. In order to get a more accurate prediction of the surface properties than in the present study, the grain boundaries need to be included in the material definition of the calculation routine. By the use of numerical calculation in general, the efforts of the process development can be reduced by numerical predictions. It enables automated virtual parameter studies and optimization routines can be applied. The presented predictive simulation can be seen as door opener to apply machine learning and optimization algorithms for process development in USP laser ablation.

Declaration of Competing Interest

The authors declare that they have no known competing financial interests or personal relationships that could have appeared to influence the work reported in this paper.

Acknowledgements

The authors want to thank the Swiss Commission of Technology and Innovation for the financial support. The opportunity to use the laboratory infrastructure at inspire AG is gratefully acknowledged.

References

[1] W. Perrie, A. Rushton, M. Gill, P. Fox, W. O'Neill, Femtosecond laser microstructuring of alumina ceramic, Appl. Surf. Sci. 248 (2005) 213–217.
[2] D. Ashkenasi, M. Lorenz, R. Stoian, A. Rosenfeld, Surface damage threshold and structuring of dielectrics using femtosecond laser pulses: the role of incubation, Appl. Surf. Sci. 150 (1999) 101–106.
[3] S.H. Kim, I.-B. Sohn, S. Jeong, Ablation characteristics of aluminum oxide and nitride ceramics during femtosecond laser micromachining, Appl. Surf. Sci. 255 (2009) 9717–9720.
[4] P. Boerner, M. Hajri, N. Ackerl, K. Wegener, Experimental and theoretical investigation of ultrashort pulsed laser ablation of diamond, J. Laser Appl. 31 (2019) 022202.
[5] M.V. Shugaev, C. Wu, O. Armbruster, A. Naghilou, N. Brouwer, D.S. Ivanov, T.J.-Y. Derrien, N.M. Bulgakova, W. Kautek, B. Rethfeld, L.V. Zhigilei, Fundamentals of ultrafast laser–material interaction, MRS Bull. 41 (2016) 960–968.
[6] D. Gilbert, M. Stoesslein, D. Axinte, P. Butler-Smith, J. Kell, A time based method for predicting the workpiece surface micro-topography under pulsed laser ablation, J. Mater. Process. Technol. 214 (2014) 3077–3088.
[7] H. Kawakami, S. Nabetani, M. Ueda, Y. Ogawa, K. Yamazaki, H. Aoyama, Simulation Method on Three-Dimensional Shape Generation Process by Femtosecond Laser Ablation, Procedia CIRP 95 (2020) 921–926.
[8] J.M. Liu, Simple technique for measurements of pulsed Gaussian-beam spot sizes, Opt. Lett. 7 (1982) 196–198.
[9] Y. Jee, M.F. Becker, R.M. Walser, Laser-induced damage on single-crystal metal surfaces, JOSA B 5 (1988) 648–659.
[10] S. Nolte, C. Momma, H. Jacobs, A. Tünnermann, B.N. Chichkov, B. Wellegehausen, H. Welling, Ablation of metals by ultrashort laser pulses, JOSA B 14 (1997) 2716–2722.
[11] P.T. Mannion, J. Magee, E. Coyne, G.M. O'Connor, T.J. Glynn, The effect of damage accumulation behaviour on ablation thresholds and damage morphology in ultrafast laser micro-machining of common metals in air, Appl. Surf. Sci. 233 (2004) 275–287.
[12] Y. Hirayama, M. Obara, Heat-affected zone and ablation rate of copper ablated with femtosecond laser, J. Appl. Phys. 97 (2005) 064903.
[13] J. Byskov-Nielsen, J.-M. Savolainen, M.S. Christensen, P. Balling, Ultra-short pulse laser ablation of metals: threshold fluence, incubation coefficient and ablation rates, Appl. Phys. A 101 (2010) 97–101.
[14] A. Rosenfeld, M. Lorenz, R. Stoian, D. Ashkenasi, Ultrashort-laser-pulse damage threshold of transparent materials and the role of incubation, Appl. Phys. A 69 (1999) S373–S376.
[15] D. Ashkenasi, R. Stoian, A. Rosenfeld, Single and multiple ultrashort laser pulse ablation threshold of Al2O3 (corundum) at different etch phases, Appl. Surf. Sci. 154–155 (2000) 40–46.
[16] G. Eberle, C. Dold, K. Wegener, Laser fabrication of diamond micro-cutting tool-related geometries using a high-numerical aperture micro-scanning system, Int. J. Adv. Manuf. Technol. 81 (2015) 1117–1125.
[17] O. Suttmann, J. Duesing, L. Overmeyer, Phenomenological model for prediction of complex ablation geometries in metal films using ultrashort laser pulses, J. Laser Appl. 28 (2016) 022208.
[18] J. Furmanski, A.M. Rubenchik, M.D. Shirk, B.C. Stuart, Deterministic processing of alumina with ultrashort laser pulses, J. Appl. Phys. 102 (2007) 073112.
[19] B. Neuenschwander, G.F. Bucher, G. Hennig, C. Nussbaum, B. Joss, M. Muralt, S. Zehnder, U.W. Hunziker, P. Schütz, Processing of dielectric materials and metals with PS laserpulses, Int. Congress Appl. Lasers Electro-Opt. 2010 (2010) 707–715.
[20] M. Hajri, P. Boerner, K. Wegener, An industry-relevant method to determine material-specific parameters for ultra-short pulsed laser ablation of cemented carbide, Procedia CIRP 74 (2018) 709–713.
[21] P. Boerner, M. Hajri, T. Wahl, J. Weixler, K. Wegener, Picosecond pulsed laser ablation of dielectric rods: Angle-dependent ablation process model for laser micromachining, J. Appl. Phys. 125 (2019) 234902.
[22] B. Neuenschwander, B. Jaeggi, M. Schmid, V. Rouffiange, P.-E. Martin, Optimization of the volume ablation rate for metals at different laser pulse-durations from ps to fs, in: Laser Applications in Microelectronic and Optoelectronic Manufacturing (LAMOM) XVII, vol. 8243, International Society for Optics and Photonics, 2012, p. 824307.
[23] J. Han, O. Malek, J. Vleugels, A. Braem, S. Castagne, Ultrashort pulsed laser ablation of zirconia-alumina composites for implant applications, J. Mater. Process. Technol. 299 (2022) 117335.